Evolution of defects in titanium grade 2 under Ti^{2+} ion irradiation

E. JOUANNY*,†,‡, S. DORIOT†, J. MALAPLATE†, M. DEHMAS‡, L. ALLAIS§, M. LE THUAUT* & T. MILLOT*

*DCNS Research/CESMAN, Centre Grand Nantes – Technocampus Océan, 44340 Bouguenais, France

†DEN-Service de Recherches Métallurgiques Appliquées, CEA, Université Paris-Saclay, 91191 Gif-sur-Yvette, France

‡Institut Jean Lamour – SI2M, CNRS UMR 7198, Université de Lorraine, 54011 Nancy CEDEX, France

§DEN-Département des Matériaux pour le Nucléaire, CEA, Université Paris-Saclay, 91191 Gif-sur-Yvette, France

Key words. Charged particle irradiations, dislocation loops, image analysis, irradiation defect evolution, titanium, transmission electron microscopy.

Summary

The complexity and diversity of microstructure involved in titanium alloys make it rather difficult to quantitatively describe defect evolution due to irradiation. This paper focuses on defect evolutions of commercially pure titanium grade 2 under Ti^{2+} ion irradiation considering the effect of dose (0.6 and 3 dpa), temperature (300°C and 430°C) and flux (15:1 ratio). An irradiation damage profile was predicted using SRIM software to obtain a homogeneous damage on at least 500 nm depth for TEM observations and simulated using JANNUS-Saclay facility. The details regarding the quantification methodologies of the defects from dark field images are provided, as are the origins of the associated uncertainties. In addition to a tangled dislocation network, presence of the <a>-type and <c>-component loops is observed. The latter was scarcely reported in the literature in the case of titanium alloys. At low temperature, the size distribution of the <a>-type dislocation loops remained similar regardless of the dose and flux whereas these parameters have highly influence at 430°C. A widening of the size distribution and an increase of the threshold incubation dose (TID) was noted with the temperature. In the case of the <c>-component loops, it was shown that the nucleation occurred in spite of the 0.6 dpa low dose.

Introduction

Owing to its good mechanical strength under irradiation, its good corrosion resistance, the 304L stainless steel is widely used as material for internal structures in the core of reactors. However, its applications in the nuclear field are often constrained. Thus, significant gains in the decrease in activation to facilitate maintenance operations, dismantling and recycling facilities, in corrosion resistance and in the reduction of the structure mass are expected. In that frame, titanium and its alloys are considered to have a great potential as nuclear structure materials with good corrosion resistance and high strength-to-density ratios after solution and aging heat treatment. For this reason, the study of the microstructural evolution of the titanium alloys under irradiation is of active interest.

In hcp materials, different types of defects are encountered during irradiation that are black dots (small clusters of point defects), dislocations and dislocation loops. The nucleation of these irradiation defects is directly related to the crystal symmetry. Habit planes of dislocation loops are usually $\{10\bar{1}0\}$ and (0001) and Burgers vector are $\frac{1}{3}\langle 1\bar{2}10\rangle$ (<a>-type dislocation loops) and $\frac{1}{6}\langle 20\bar{2}3\rangle$ (<c>-component loops), respectively. It is commonly admitted that <a>-type dislocation loops are interstitial in character whereas <c>-component loops are vacancy-type defects (Griffiths, 1991). <a>-type vacancy loops were nevertheless observed in titanium and zirconium alloys (Griffiths, 1988, 1991; Woo, 2000). Nature and habit planes of dislocation loops are highly dependent on the c/a ratio of the structure and on the amount of alloying elements of the considered material (Griffiths, 1991, 1993a). In the case of pure titanium ($c/a < 1.732$), prism plane loops appear preferentially whereas the loops are located in basal planes for hcp materials with $c/a > 1.732$. The increase of impurities in solid solution (Griffiths, 1991) or the presence of internal stresses (Griffiths, 1988) tend to increase the probability of basal plane loop formation by increasing the c/a ratio when it is below 1.732. The irradiation-induced defects have a strong influence on the mechanical properties. As an example, it was shown that their presence after neutron irradiation confers to titanium alloys improved yield strength accompanied by a loss of tensile ductility (Kozhevnikov *et al.*, 1999a). The nature, size and density of radiation-induced defects were found to be important parameters governing the in-reactor behaviour of the material. Indeed, the presence of <a>-type dislocation loops and black dots induces material

Correspondence to: E. Jouanny, DCNS Research/CESMAN, Centre Grand Nantes – Technocampus Océan, Rue de l'Halbrane, 44340 Bouguenais, France. e-mail: emilie.jouanny@cea.fr

Table 1. Nominal chemical composition of the CP Ti grade 2 (in wt%).

Elements	Ti	Fe	C	O	N
	bal.	0.02	0.006	0.17	0.003

hardening and affect strongly the mechanical properties. <c>-component loops are responsible for the growth phenomenon that is a dimensional change of the material: elongation along the <a>-axis and shortening along the <c>-axis (Griffiths, 1988; Onimus & Béchade, 2012). However, for a better understanding and a further modelling of mechanical behaviour taking account of the characteristics of the irradiation-induced defects, it appears necessary to identify and quantify these defects after irradiation. This consideration prompted the present study that is focused on the effects of irradiation parameters (temperature, dose and flux) on the presence, size, density and nature of radiation-induced defects, in a model material that is a single-phase CP titanium: CP Ti grade 2. For this purpose, ion irradiations were conducted in the JANNUS French platform (Joint Accelerators for Nanosciences and Nuclear Simulation) to simulate neutron irradiation damage. Quantification of defects was carried out thanks to image analysis of TEM (Transmission Electron Microscopy) images. Method of counting defects is given and mechanisms of appearance of defects are discussed.

Materials and experimental procedures

The considered material is a commercially pure α-titanium (CP Ti grade 2). This material was provided by TIMET Savoie, France under the shape of 100 mm in diameter bars. The nominal chemical composition (in wt%) of the as-received material is given in Table 1. It can be noticed that the interstitial elements (impurity) greatly impact the transus beta temperature. The determination of substitutional solute elements was carried out by Inductively Coupled Plasma (ICP) analysis. Combustion and infrared absorption measurement, fusion hot extraction, reducing molten in a nickel bath and determination by infrared absorption, were used for C, O, N, respectively.

After hot forming, CP Ti grade 2 was annealed for 2 h at 675°C and then air cooled. The resulting microstructure consists of equiaxed α grains with a mean equivalent diameter of 60 μm (Fig. 1).

For irradiation and further TEM observations, disk specimens with a diameter of 3 mm and a thickness of 100 μm were machined from the as-received state. Then, the samples were prepared by electropolishing (twin jet electrolytic thinning) to reduce the thickness until less than 50 μm, before subjecting them to the irradiation. Only one face was polished at this step. To do that, two disks are put together back to back and the resulting samples have one face polished and the second one unpolished. The irradiation was carried out on the polished face. After irradiation, the disk is thinned again to obtain a hole at the centre of the disk by electropolishing on the nonirradiated face only (backpolishing). The irradiated face was protected using Lacomit varnish. No surface layer of the irradiated face has been removed. An electrolyte containing 10% perchloric acid and 90% ethanol, at –10°C and 30 V was used. The disk specimens were irradiated using Ti^{2+} ions from the JANNUS French platform. Ion irradiations were realized for their easiest utilization compared to neutron irradiation (no sample activation, faster irradiation, and more flexibility on the parameter choices) and lower cost. The JANNUS facility is equipped with three electrostatic accelerators (Epiméthée, Pandore and Japet) and a triple beam chamber (Beck *et al.*, 2015). The irradiation were performed using the 2 MV Tandem Pelletron JAPET^{TM} (Saclay, France) (Serruys *et al.*, 2009; Beck *et al.*, 2015).

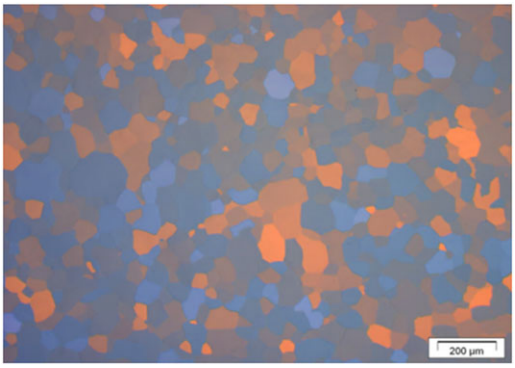

Fig. 1. Equiaxed microstructure of the as-received CP Ti grade 2. Observation with polarized light.

Figure 2 shows the triple beam chamber and the heating sample holder used for the irradiations. The heating sample holder located in the triple beam chamber can accommodate up to 19 disk samples and is capable of elevating the sample temperature up to 850°C. The sample temperature was measured by a K-type thermocouple welded at the surface of the sample. The choice of the ions, temperatures and doses will be presented in *Results and discussion* section.

During the irradiation, the implanted Ti concentration is estimated by measuring the beam current every 10 min for 30 s with a movable device of multi-Faraday cups (going up and down by the entry indicated by the cross on Fig. 2A).

The irradiated samples (Fig. 2B) were then observed by TEM in order to identify the type of dislocation loops and their evolution with irradiation conditions. The TEM examinations were conducted using a 200 kV Jeol 2100 microscope. These examinations were focused on the microstructural evolution of CP Ti grade 2 samples under irradiation. As mentioned in the literature (Griffiths, 1993a; Woo, 2000), <a>-type and <c>-component loops can be nucleated readily under irradiation in hcp structure. Consequently, particular attention

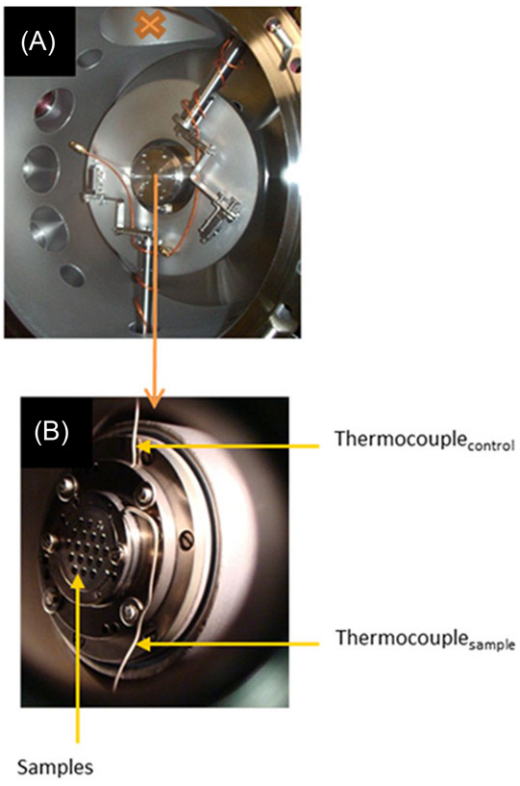

Fig. 2. (A) Triple beam chamber and (B) heating sample holder with thermocouples.

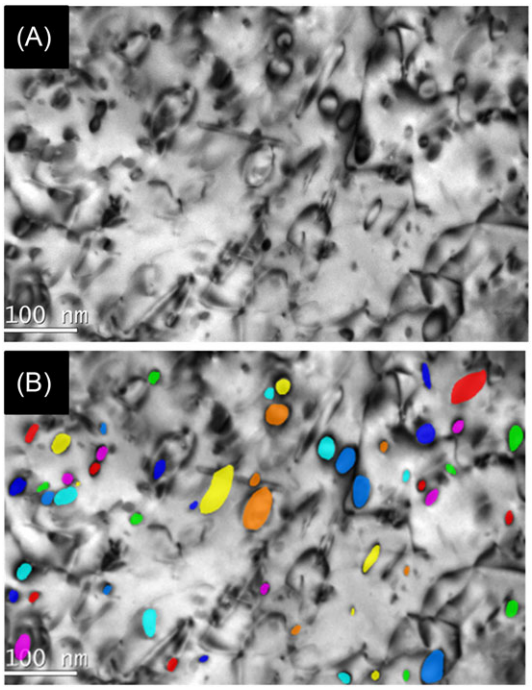

Fig. 3. Illustration of the counting of <a>-type dislocation loops in CP Ti grade 2 after irradiation: (A) original bright field image showing <a>-type dislocation loops and (B) after drawing defects on the graphic tablet – use of the Visilog software. Coloured shapes correspond to the drawing defects (here, <a>-type dislocation loops) considered on this micrograph. Different colours were used for better visualization.

was paid to the identification of these loops. Complete characterization of loops was not carried out but the presence of two families of loops was checked according to the well-known Burger vectors in hcp metals ($\frac{1}{3}\langle 1\bar{2}10\rangle$ (<a>-type dislocation loops) and $\frac{1}{6}\langle 20\bar{2}3\rangle$ (<c>-component loops)). Using reflector $g = 0002$, observable loops are <c>-component loops and as some loops, that are visible in $g = 10–11$ but are invisible under these conditions, <a>-type dislocation loops are also present in the materials. For <a>-type loop imaging, a 10–11 diffracting vector was used near the prism foil zone axis $B = [1–210]$. In this last case, only 2/3 of loops will be in Bragg conditions and visible on the micrographs. Consequently, the number density will be given by taking into account a corrective factor of 3/2 to compensate for these missing loops. For <c>-component loop imaging, a prism-plane foil orientation and a 0002 diffracting vector were used to image the <c>-component loops. Consequently, the <c>-component loops are imaged edge-on and appear as short segments. However, to facilitate the counting especially when the <c>-component loops were very 'wavy' in the 0002 diffracting conditions and to observe the stacking faults of the <c>-component loops, 10–11 diffracting vector was used near the prism foil zone axis $B = [1–210]$. The defect distributions were counted by image analysis, using the Noesis Visilog software™. An example of <a>-type loop counting is given in Figure 3. After selecting area on the micrograph, defects are selected and defined manually with a graphic tablet and thus automatically counted and measured. It can be noticed that the influence of the overlapping of defects and truncation by foil surface can be neglected for <a>-type dislocation loops.

Most of the counting was achieved on bright field images only. But the recording of both bright field and weak beam images was sometimes realized (Fig. 4). This method is more difficult to implement but the edges of the loops are better defined. The merit of the weak beam technique is illustrated in Figure 4(B). Although bright field image leaves the exact position of the dislocation loops, the weak beam image displays a clear dislocation contrast. Then, these two complementary observations allow minimizing confusions on the nature of the defects. For instance, weak beam micrograph (Fig. 4B) confirms that the features arrowed in Figure 4(A) are not black dots but loops, that are ellipses with a sharp contour. Besides, in (Fig. 4B), circles show hydrides that were not clearly observable in bright field (Fig. 4A).

For <c>-component loops, the 'linear density' was measured. This parameter was obtained by measuring and summing up the lengths of the segments corresponding to the loops on the micrographs ($g = 0002$) and is expressed in $m.m^{-3}$.

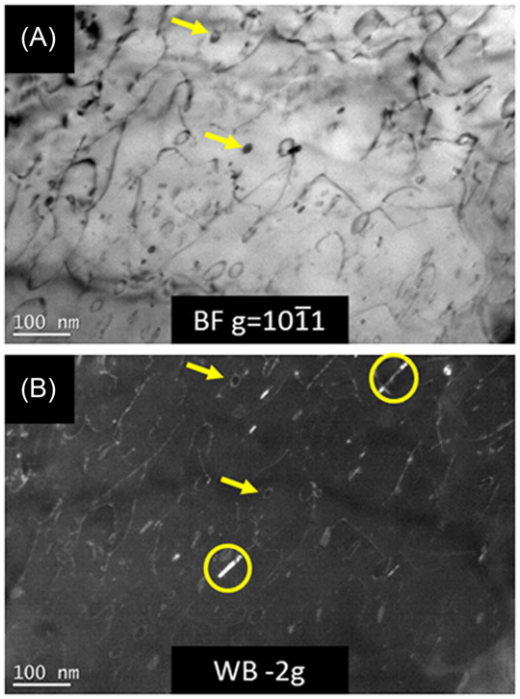

Fig. 4. TEM observations of <a>-type dislocation loops and hydrides in CP Ti grade 2: (A) bright field and (B) weak beam using $-2g$. Arrows evidence <a>-type dislocation loops and circles show hydrides, not clearly observable in bright field image.

The quantitative analyses of the defects have been done in several α grains in order to increase the counting statistics. Because the grain size is large compared to the observable area of a thin foil, several locations in the same grain will be also taken into account. For each condition, the counting statistics have been done on several hundred of defects. The thin foil thickness of the considered location was measured by EELS (Electron Energy Loss Spectroscopy). This technique considers energy distribution of electrons which have crossed the sample. Thicker the sample, more important the incident electron energy loss. Several authors have established the link between the t/λ parameter and the ratio of plasmon peak area and zero loss peak in the energy loss distribution, where t is the thickness of the analysed zone and λ the mean free path for inelastic scattering (Crozier, 1990; Egerton, 1996; Nakafuji *et al.*, 2001; Lee *et al.*, 2002; Ohshima *et al.*, 2004; Mitchell, 2006).

Results and discussion

Irradiation conditions

At first, the choice of the irradiation ion nature and energy, thanks to damage profiles predicted using SRIM software is explained. Then, the choice of the irradiation conditions (temperatures, doses, fluxes) taking into account the constraints of the JANNUS platform and the desire to reproduce the in-service conditions is discussed.

Irradiation ion nature and energy. Titanium alloys were chosen to irradiate the CP Ti grade 2 samples in order to avoid any severe modification of their chemical composition. The choice of the incident ion energy is crucial: the higher the incident ion energy, the higher the depth of the ion implantation and consequently the more homogeneous the damage profile on the depth of interest for the study. For TEM observations, an irradiated layer of about 500 nm thick is needed. Simulations of damage profiles were done using SRIM software, and considering the energies ranging from 1 MeV to 6 MeV. The energy was found to be 6 MeV with Ti^{2+} incident ions in order to obtain a moderate gradient irradiation damage. But, the high energy ions induce the dose drops and an alternative to get higher dose near the surface is the use of degraders. Here, an aluminium foil is put at the surface of the samples inducing a shift of the damage peak towards the sample surface proportionally to its thickness (Fig. 5). Thus, a good compromise with the thickness of the irradiated layer, the homogeneity of the irradiation dose, and the dose seems to be a 6 MeV Ti^{2+} irradiation with a 0.8 μm thick Al degrader.

Irradiation flux and dose. The highest dose examined in this study was determined by the dose obtained after one day of irradiation with the highest feasible flux. This flux is estimated to be about 5×10^{11} ions cm^{-2} s^{-1} for Ti^{2+} ions and one day of irradiation corresponds to about 6 h. Indeed, a dose of about 10^{16} ions cm^{-2} ($\approx$ 3 dpa[1]) was obtained. The highest feasible flux can vary for each irradiation experiment. So, the irradiation time was adapted to maintain the same dose.

The lowest dose was chosen to be five times lower than the highest one. It means a dose of 0.6 dpa. With a dose as low as 0.6 dpa, the presence of irradiation defects can still be expected (authors have already observed irradiation defects at doses as small as 0.1 dpa; Leguey *et al.*, 2001) and noticeable differences with the 3 dpa irradiated samples could be obtained.

A low feasible flux was chosen as the lowest flux, corresponding to a ratio of about 1:15 compared to the highest flux. It permits to obtain a dose of 0.6 dpa after about 30 h.

Irradiation temperature. According to the literature (Kozhevnikov *et al.*, 1999a), hardened microstructure seems to be encountered at low irradiation temperature (< 250°C). The microstructure consists of a dense distribution of small defects. At higher temperature (> 350°C), defects are bigger and less hardening. Therefore, two irradiation temperatures have been considered. The first one is assumed to reproduce the hardened microstructure with a high density of small defects. The second one tends to reproduce the higher temperature microstructure with bigger defects. To reproduce the irradiation

[1] dpa= number of displacements per atom during the irradiation.

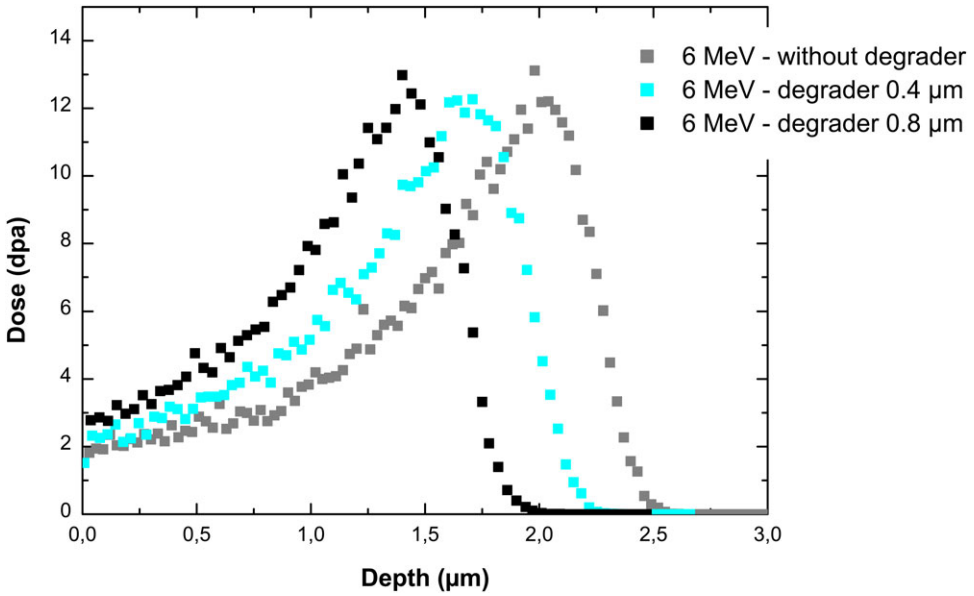

Fig. 5. Simulation of damage profile using SRIM software for Ti^{2+} ions irradiation with energy of 6 MeV and several thickness of Al degrader.

Table 2. Irradiation conditions: dose, temperature, flux and damage rate.

Dose, temperature	Flux (ions cm^{-2} s^{-1})	Damage rate (dpa s^{-1})
3 dpa 300°C high flux	7.2×10^{11}	2.2×10^{-4}
3 dpa 430°C high flux	7.7×10^{11}	2.3×10^{-4}
0.6 dpa 300°C high flux	6.5×10^{11}	1.6×10^{-4}
0.6 dpa 430°C high flux	4.4×10^{11}	1.9×10^{-4}
0.6 dpa 300°C low flux	3.1×10^{10}	7.5×10^{-6}
0.6 dpa 430°C low flux	3.6×10^{10}	8.6×10^{-6}

defects induced by neutron irradiations, ion irradiations must be performed at higher temperatures (Was, 2007; Was & Averback, 2012). Indeed, the size of the radiation-induced defects after ion irradiation is usually smaller than those observed after neutron irradiation for the same irradiation temperature. Thus, we need to use in the 'low temperature regime' a temperature high enough to simulate the microstructure obtained with neutrons between 60°C and 250°C (Griffiths *et al.*, 1983; Kozhevnikov *et al.*, 1999a), but not too high in order to avoid the 'high temperature regime' (Kozhevnikov *et al.*, 1999b; Tähtinen *et al.*, 2007). For all these reasons, the two chosen temperatures were 300°C and 430°C.

Sum up of the irradiation conditions. The irradiation conditions: dose, temperature, flux and damage rate are summarized in Table 2.

TEM investigations

Microstructures before irradiation: as-received and annealed state (430°C). Figure 6 displays the microstructure before irradiation of CP Ti grade 2. The nonirradiated state (Fig. 6A) is characterized by long screw <a>P dislocation systems ($\sim 10^{13}$ dislocations.m^{-2}) that are the most common gliding systems in hcp Ti (Wasz *et al.*, 1996). Other gliding systems

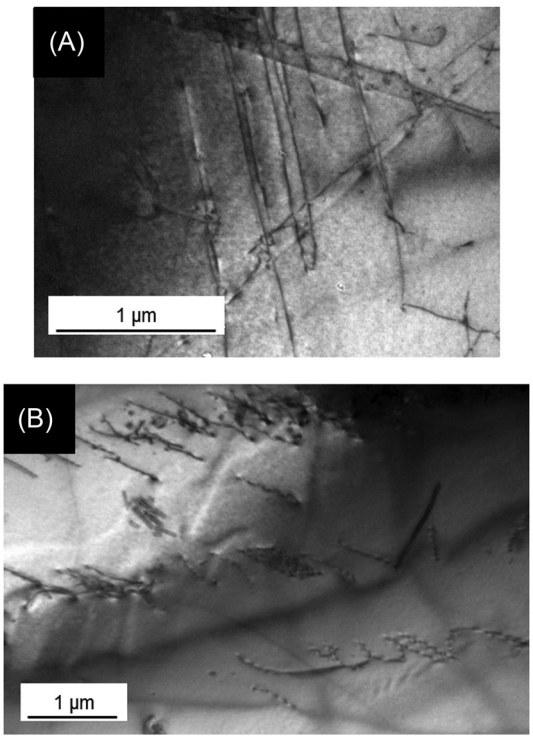

Fig. 6. Microstructure before irradiation of CP Ti grade 2: (A) micrograph near a basal orientation before irradiation, <a>P dislocation systems and (B) <a>-type dislocation pile-up. TEM observations.

Table 3. Evolution of the dislocation density for CP Ti grade 2 at the as-received state, after annealing of 6 h and after irradiation at 0.6 dpa (high flux and low flux) and 3 dpa high flux. TEM observations.

Irradiation condition	Dislocation density (dislocations.m^{-2})
As-received state (unirradiated)	$3.3 \pm 2.7 \times 10^{13}$
Annealing 6 h (unirradiated)	$0.87 \pm 0.45 \times 10^{13}$
0.6 dpa 430°C high flux	$1.2 \pm 0.66 \times 10^{13}$
3 dpa 430°C high flux	$16.7 \pm 8.6 \times 10^{13}$
0.6 dpa 430°C low flux	$6.9 \pm 1.5 \times 10^{13}$

are present and dislocation pile-up can be observed (Fig. 6B), but no <c+a> dislocation systems appear on prism-plane foil orientation micrographs. This microstructure is the result of the thermomechanical process.

Annealing at 430°C during 6 h was carried out to evaluate the effect of temperature without irradiation. The microstructure of this annealed state is similar to the as-received state but the dislocation density is divided by three (Table 3). This means that the temperature induces a recovery of the dislocations.

Influence of temperature at a dose of 3 dpa. As shown in Figure 7, the <a>-type defects evolves under irradiation. At low temperature (300°C), tangled <a> dislocations seem to be present, but are hardly observable because of the contrast of small <a>-type dislocation loops and black dots in high density. At high irradiation temperature (430°C), dislocations are still present but the screw <a>P dislocation systems are replaced by a dense ($\sim 10^{14}$ dislocations m^{-2}) tangled <a> dislocation network associated with large spaced <a>-type dislocation loops (Fig. 7B).

These observations give the evidence of the two expected microstructures and are very similar to the microstructures observed in the literature after neutron irradiations at 200°C and 400°C (Kozhevnikov *et al.*, 1999a). Thus, the irradiated sample at 300°C (Fig. 7A) does reproduce the hardened microstructure with a high density of small defects ($\sim 2 \times 10^{22}$ loops.m^{-3}, mean equivalent diameter. ~10 nm), and the irradiated sample at 430°C (Fig. 7B) reproduces the higher temperature microstructure with less numerous and less hardening bigger defects ($\sim 3.5 \times 10^{21}$ loops.m^{-3}, mean equivalent diameter ~16 nm). These resulting microstructures are the consequence of the ion-microstructure interactions. These interactions produce a great density of point defects [vacancy and self-interstitial atom (SIA)] that enhance diffusion processes. If no annihilation by mutual recombination or no loss to sinks in matrix (grain boundaries, dislocations etc.) occur, these defects migrate by a diffusional mechanism and agglomerate in bigger defects as interstitial or vacancy loops (Was, 2007; Nastar & Soisson, 2012). Dubinko *et al.* (2006) proposed a modelling to describe the evolution of loop size distribution in a pure zirconium versus dose and irradiation

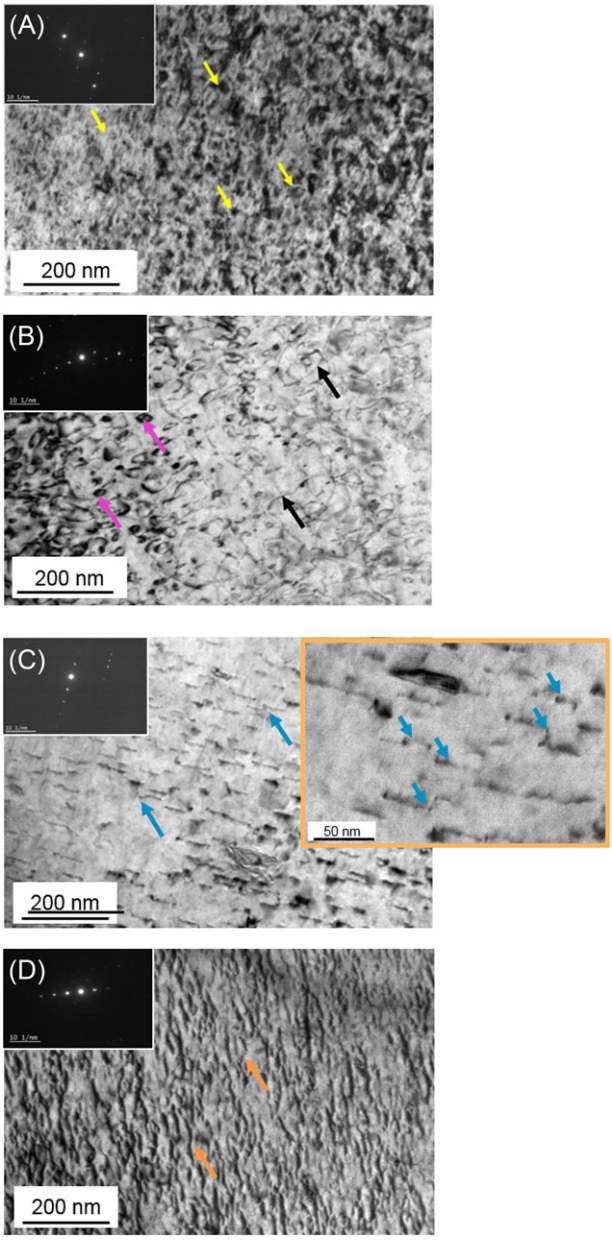

Fig. 7. Microstructure of CP Ti grade 2 after irradiation at a dose of 3 dpa: (A) 300°C <a>-type dislocation loops, (B) 430°C <a>-type dislocation loops, (C) 300°C <c>-component loops and (D) 430°C <c>-component loops. Arrows in light colour show <a>-type dislocation loops (in A and B) and dark arrow show dislocations in (B). Arrows in (C) and (D) illustrate <c>-component loops. TEM observations.

temperature. Diffusivity of the species, vacancy and SIA density, linear density of the dislocation (as sinks for the point defects) were important parameters to be taken into account. This model gives evidence of a lower loop density with a bigger size at higher irradiation temperature. Rising the irradiation temperature induces a lowering of the defect supersaturation (Nastar & Soisson, 2012), enhances mutual recombination or

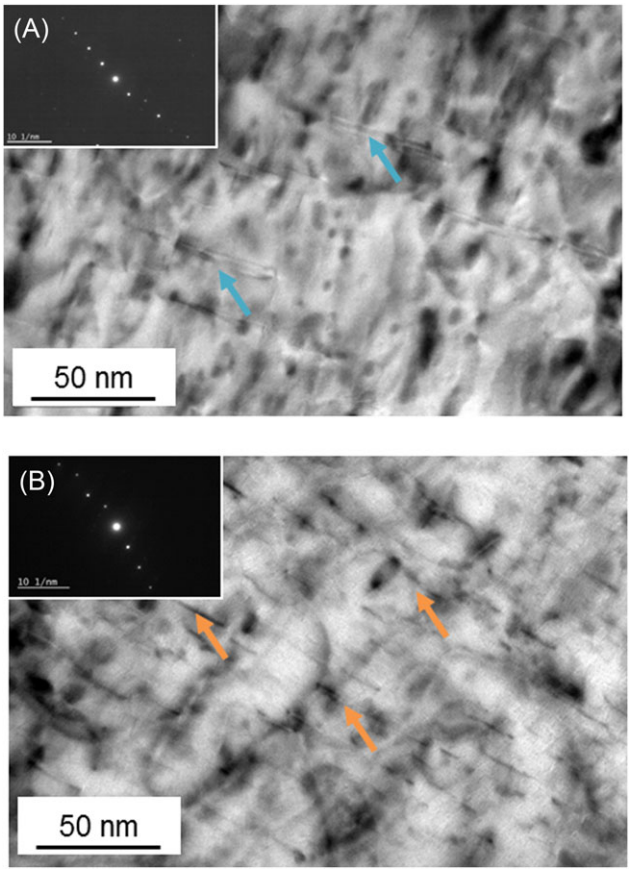

Fig. 8. <c>-component loops observed in $g = 10–11$ and B~[1–210] for samples irradiated at 3 dpa: (A) 300°C and (B) 430°C. Arrows show <c>-component loops with stacking fault (A) or without stacking fault (B). TEM observations.

Table 4. Number of counted <a>-type dislocation loops and considered grains in each irradiation condition (both the <a>-type and <c>-component loops).

Irradiation condition	<a>-type loops	<c>-component loops
3 dpa 300°C high flux	2322 – 5 grains	285 – 6 grains
0.6 dpa 300°C high flux	2014 – 6 grains	248 – 5 grains
0.6 dpa 300°C low flux	938 – 2 grains	472 – 4 grains
3 dpa 430°C high flux	1087 – 3 grains	380 – 2 grains
0.6 dpa 430°C low flux	1070 – 4 grains	788 – 2 grains

annihilation to the sinks thank to faster diffusion processes (Griffiths *et al.*, 1983) and thus reduces the loop nucleation incidence. In addition, it enhances the diffusivity of the species and promotes loop growth. Our experimental data are in agreement with the model proposed by Dubinko *et al.* (2006) since the density of <a>-type loops is divided by about 5 and the size is multiplied by about 2 in the irradiation at 430°C as compared to the irradiation at 300°C.

Whereas no <c>-component defects can be seen in prism foil orientation before irradiation, a big density of <c>-component defects is observed in irradiated samples. They appear after irradiation at 300°C as straight short segments parallel to the basal plane traces in prismatic orientations (Fig. 7C) with the 0002 reflector (edge-on view) and are known to be basal <c>-component loops with $\frac{1}{6}\langle 20\bar{2}3\rangle$ Burger vector (Griffiths, 1988, 1991). Some steps arrowed Figure 7(C) can be seen on these straight line defects and could be the sign of climbs of these loops, as previously observed by Griffiths in Zr-alloys (Griffiths, 1993b). The linear density is very high and close to 2×10^{14} m.m^{-3}. The mean size of these basal defects is difficult to determine precisely because the steps make the measure difficult to manage, but has been estimated to be around 100 nm. These basal defects appear after irradiation at 430°C as well (Fig. 7D), but their straightness is not so obvious. This phenomenon is probably due to an enhancement of the loop climbing with the temperature: climb is due to vacancy absorption (Griffiths, 1993b) that is promoted by the faster diffusion of vacancies at higher temperature. In thin foil orientation with the 10–11 reflector near the [1–210] zone axis, their stacking fault is clearly observable as Moiré fringes after irradiation at 300°C (arrowed in Fig. 8A), as previously observed in Zr alloys (Gilbon & Simonot, 1994; Simonot, 1995). The <c>-component loops seem to be defaulted after irradiation at 430°C (their contrast in Fig. 8B appears as straight-line without Moiré fringes). Such defaulted loops were observed in Zircaloy-4 alloy when an annealing was carried out after irradiation (Gilbon & Simonot, 1994). For both irradiation temperatures (Fig. 8), the <c>-component defects appear similar in size and density. The apparent higher density for the irradiation at 430°C is due to the higher thin foil thickness (200 nm instead of 100 nm). The waving aspect of the <c>-component loops after irradiation at 430°C makes their counting very difficult to manage. Therefore, an additional measure of the linear density and size of <c>-component loops in both conditions was carried out in the 10–11 reflecting conditions. It gives a quite similar result for both irradiation conditions.

These microstructural features are commonly observed in Zr-based alloys at high doses with neutron, proton and ion irradiations (Northwood *et al.*, 1979; Griffiths, 1988; Hengstler-Eger *et al.*, 2012; Yan *et al.*, 2015) but were scarcely reported in the literature in the case of titanium alloys (Griffiths *et al.*, 1983). As discussed by Woo (1988), the growth of <c>-component loops is well understood in the frame of the DAD (Diffusion Anisotropy Difference) model. Because of the higher mobility of SIAs in the basal plane rather than along the *c* axis (and the isotropic diffusion of vacancies), dislocations parallel to the *c* axis will absorb a net flux of SIAs, whereas dislocations in the basal plane will absorb a net flux of vacancies (Onimus & Béchade, 2012). The DAD was not demonstrated but this mechanism therefore explains why the basal vacancy loops can grow.

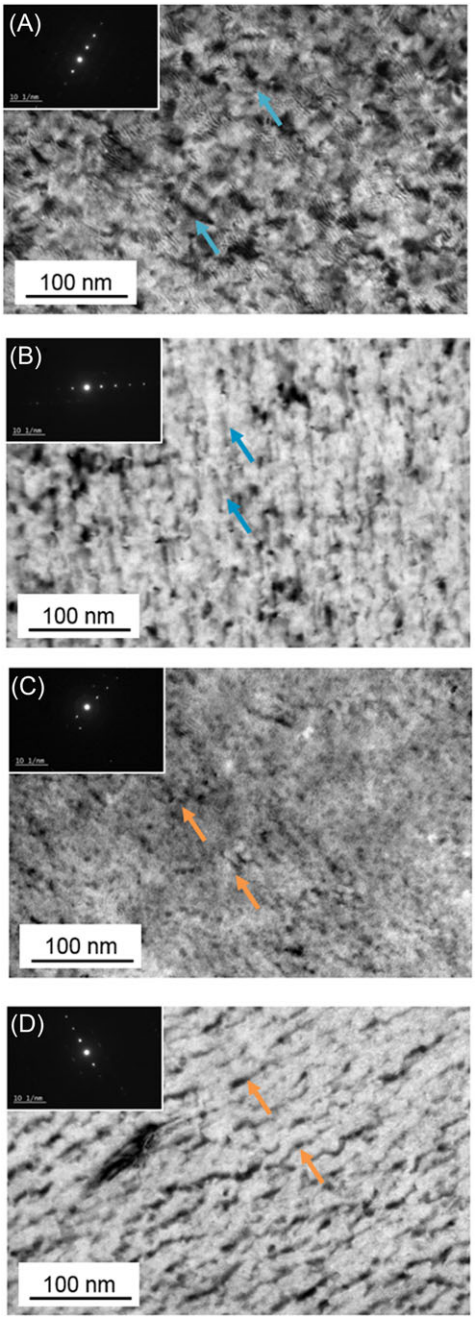

Fig. 9. <c>-component loop microstructure of CP Ti grade 2 irradiated at 300°C: (A) 0.6 dpa high flux and (B) 0.6 dpa low flux and at 430°C: (C) 0.6 dpa high flux and (D) 0.6 dpa low flux. Arrows show <c>-component loops. The observable fringes are not due to stacking fault but correspond to Moiré fringes due to surface contamination. TEM observations.

Influence of dose and flux. The evolutions of the defect microstructure with the dose and flux have been described and quantified for the two irradiation temperatures. The exact number of analysed loops in each irradiation condition is given in Table 4. Dislocations have been also quantified for the irradiations carried out at 430°C. At 300°C, the dislocations are not quantified because it is difficult to precisely count them due to the high density of <a>-type dislocation loops.

Table 5. Number density of <c>-component loops in CP Ti grade 2 irradiated at 300°C.

Irradiation condition	Linear density ($m.m^{-3}$)
3 dpa 300°C high flux	$2.1 \times 10^{14} \pm 0.6 \times 10^{14}$
0.6 dpa 300°C high flux	$1.3 \times 10^{14} \pm 0.9 \times 10^{14}$
0.6 dpa 300°C low flux	$1.9 \times 10^{14} \pm 0.7 \times 10^{14}$

Table 6. Number density and mean equivalent diameter of <a>-type dislocation loops in CP Ti grade 2 irradiated at 300°C and 430°C.

Irradiation condition	Number density ($loops.m^{-3}$)	Mean equivalent diameter (nm)
3 dpa 300°C high flux	$1.9 \pm 0.3 \times 10^{22}$	9 ± 3
0.6 dpa 300°C high flux	$1.3 \pm 0.5 \times 10^{22}$	7 ± 2
0.6 dpa 300°C low flux	$1.6 \pm 0.5 \times 10^{22}$	9 ± 2
3 dpa 430°C high flux	$3.6 \pm 0.8 \times 10^{21}$	17 ± 8
0.6 dpa 430°C high flux	0	–
0.6 dpa 430°C low flux	$6.6 \pm 2.5 \times 10^{21}$	35 ± 20

In the case of the irradiations at 300°C, <a>-type and <c>-component loops observed at a dose of 0.6 dpa high and low flux (Figs. 9A–C) are similar to those obtained at a dose of 3 dpa high flux (Figs. 7A–C). This similitude is confirmed by the quantitative measurement of the number density and the mean size of these defects (Tables 5 and 6) as well as the size distribution for <a>-type dislocation loops (Fig. 11). It is noted in Table 5 a smaller linear density of <c>-component loops at a dose of 0.6 dpa high flux when compared with the dose of 3 dpa high flux, but with a significant spread of the measurement in the considered grains (0.6 dpa condition). The scattering could be an artefact of the measure but this result is consistent with the literature. Usually a higher density and a more homogeneous distribution of the <c>-component loops is observed with a higher dose (Gilbon *et al.*, 2000; Tournadre *et al.*, 2012; Doriot *et al.*, 2014) in Zr-alloys. The nearly absence of dose-rate and dose influence is not surprising for <a>-type dislocation loops. The irradiation conditions seem to correspond to the ž low-temperature [a] regime (Zinkle *et al.*, 1993; Zinkle, 2012) where the defects are not very mobile and the dislocation networks are nearly independent of the irradiation temperature. According to these authors, in the 'low temperature regime', the microstructure is relatively insensitive to variations in the damage rate and reaches a saturation level at a relatively low dose, as seen here. A lowering in the dose rate is usually considered as equivalent to a rise in the irradiation temperature in the literature. Mansur (Mansur, 1978) proposed an analytic expression to estimate the shift in temperature due to the damage-rate difference. A shift in temperature of about 50°C for a ratio in a dose rate 15:1 at 300°C was found. In

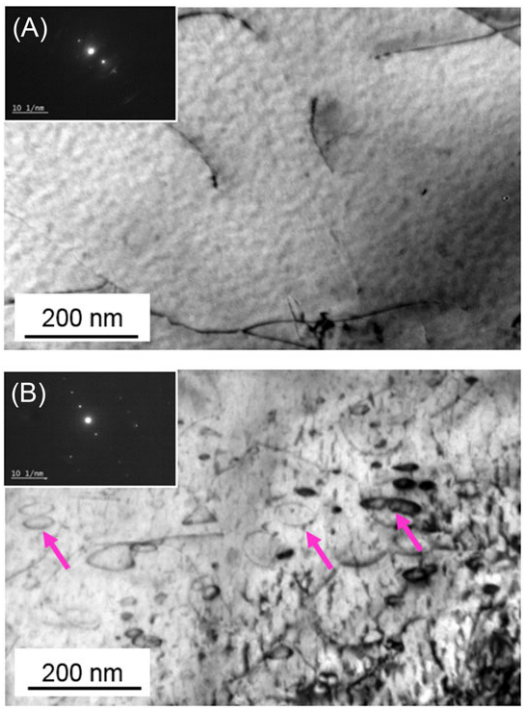

Fig. 10. <a>-type dislocation loops in CP Ti grade 2 irradiated at 430°C: (A) 0.6 dpa high flux and (B) 0.6 dpa low flux. Arrows show <a>-type dislocation loops. TEM observations.

the low temperature regime, such a difference in irradiation temperature could not induce observable differences in the microstructure.

The most surprising feature in these observations is the presence of such a high density of <c>-component loops at such a low dose. <c>-component loops were almost never reported in the literature in the case of titanium alloys (Griffiths, 1993a) and were usually observed at doses higher than 3 dpa and with a much lower linear density in Zr-alloys, after proton, ion or neutron irradiation (Tournadre *et al.*, 2012). This phenomenon could probably be partially explained by the adsorbed hydrogen into the material before and during irradiation, that is suspected to enhance the nucleation of the <c>-component loops (Tournadre *et al.*, 2013). The hydrogen adsorption in CP Ti grade 2 is evidenced by the presence of a large quantity of hydrides not shown here.

In the case of the irradiations at 430°C (Fig. 10), there appear noticeable differences in the <a>-type dislocation loops and in the dislocations observed at a dose of 0.6 dpa high and low flux and at a dose of 3 dpa high flux (Fig. 7B). For the dose of 0.6 dpa high flux, no <a>-type dislocation loops can be seen[2] (Fig. 10A). The observed microstructure is similar to the one of as-received state characterized by straight dislocation network. It must be emphasized that in this irradiation condition (1 h 30 min), the dislocation density is lower than after 6 h annealing. Thus, irradiation accelerates the recovery of initial dislocation network. However, numerous <a>-type dislocation loops and tangled dislocation network are present both after irradiation at 3 dpa high flux and 0.6 dpa low flux (with a flux 15 times lower). This is illustrated by the micrographs given in Figures 7(A) and 10(B), and the resulting quantification results reported in Table 6 and in Figure 12. Arrows in Figures 7 and 10 show examples of dislocation loops in each irradiation conditions.

The absence of <a>-type dislocation loops at 0.6 dpa high flux, at the temperature of 430°C, was unexpected, especially as they were present for the same dose at 300°C. This can be explained at least partially by the difference of temperature regime. According to the literature (Zinkle *et al.*, 1993; Zinkle, 2012), in the high temperature regime, dislocations could be sinks for irradiation point defects and could delay the loop occurrence because the diffusion effect is not negligible at this temperature. Consequently, it appears necessary to recover the initial dislocation microstructure before the formation of loops. This phenomenon of dislocation network restoration has already been mentioned in the literature in case of stainless steels (Pokor *et al.*, 2004; Garner, 2012; Renault-Laborne *et al.*, 2015). At 300°C, it is not the case because the defects are less mobile and can't move to sinks.

We can wonder why a lowering of the flux reduces the delay of <a>-type dislocation loop occurrence. Recovery of the initial dislocation network has probably occurred before the end of irradiation at low flux (irradiation time = 30 h) and the formation of <a>-type dislocation loops is thus possible. At high flux 430°C 0.6 dpa, the irradiation time of 1 h 30 min is not sufficient to obtain complete restoration of the initial dislocation network.

In addition, it is noted that the size of <a>-type dislocation loops is higher and the widening of the size distribution is larger at 0.6 dpa low flux than at 3 dpa high flux. Therefore, the influence of the temperature on <a>-type dislocation loops is similar at low flux and at high flux (i.e. an increase of size associated with a decrease of density), but this influence seems higher at low flux than at high flux (comparison between 0.6 dpa low flux at 300°C and 430°C with 3 dpa high flux at 300°C and 430°C). This comparison is realized between different doses because no loops are observed at the 0.6 dpa high flux. Nevertheless, in a first approximation, the difference in fluxes may partly explain the stronger effect of temperature at low flux. Indeed, a coupling between flux and temperature to obtain a given microstructure is evidenced in the literature (Mansur, 1978; Was, 2007; Was & Averback, 2012). For the same temperature, lowering the flux should lead to a microstructure representative of a higher irradiation temperature. In a high temperature regime, increasing the temperature gives a decrease in <a>-type dislocation loop density and increase in the loop size.

[2] This result was checked on several samples of the same irradiation campaign and on a sample of a second irradiation campaign in the same conditions.

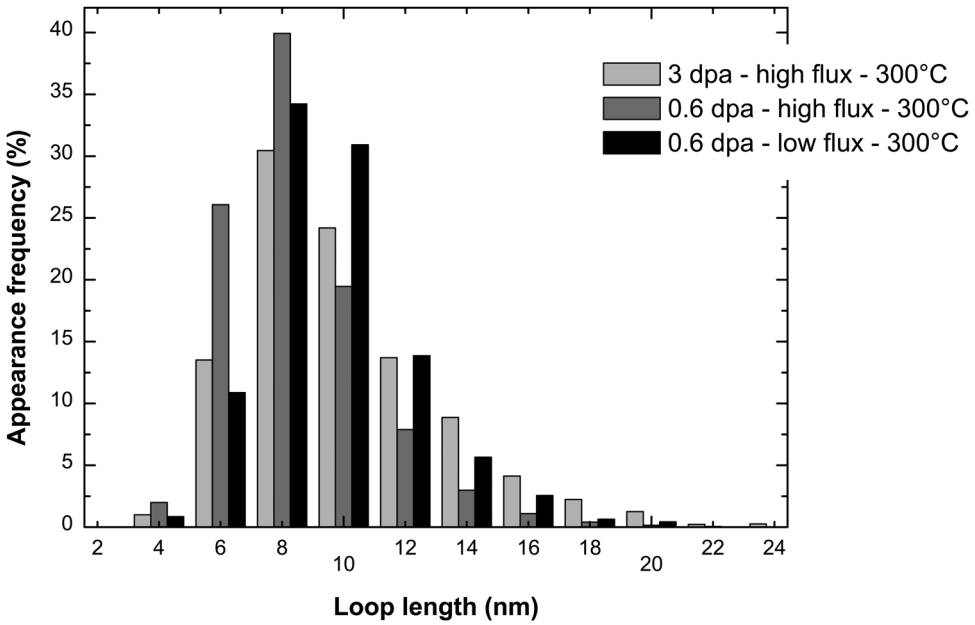

Fig. 11. Size distribution of <a>-type dislocation loops in CP Ti grade 2 irradiated at 300°C for dose of 0.6 dpa (high and low flux) and 3 dpa high flux.

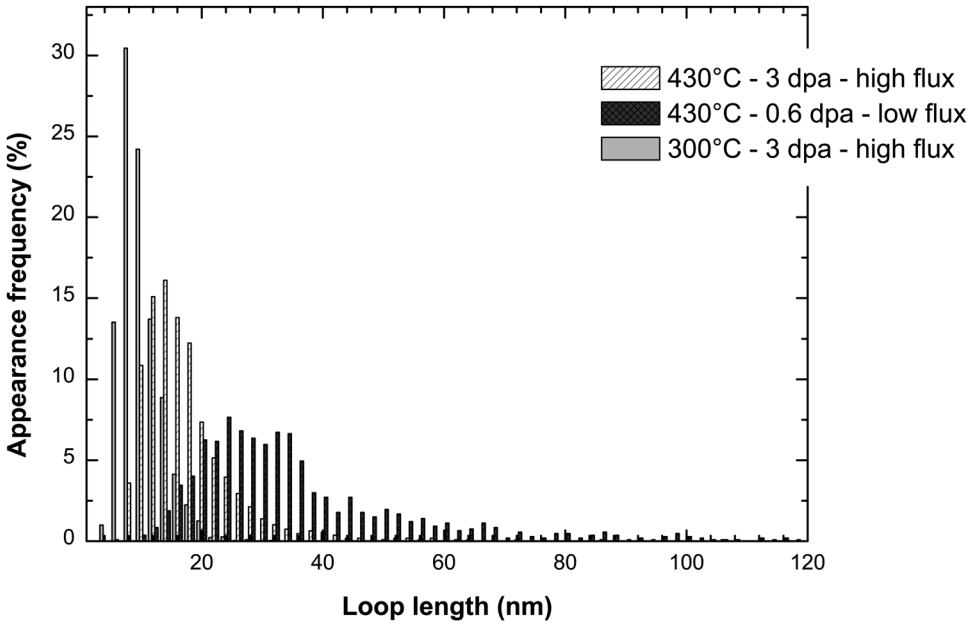

Fig. 12. Size distribution of <a>-type dislocation loops in CP Ti grade 2 irradiated at 430°C for dose of 0.6 dpa low flux and 3 dpa high flux compared to 3 dpa 300°C.

The <c>-component dislocation loops are also observed for irradiation at 430°C. Figures 7(D), 9(C) and (D) display the microstructures observed at a dose of 3 dpa high flux, 0.6 dpa high flux and 0.6 dpa low flux, respectively. For all cases, the shape of the <c>-component loops presents a wavy aspect. For the irradiation conditions, 0.6 dpa high flux, smaller and less numerous <c>-component loops are hardly observable (Fig. 9C). It can be concluded that the effect of dose on the <c>-component defects is expressed, as for <a>-type defects, by a higher delay of occurrence at 430°C compared to 300°C. In Zr-alloys, the delay of occurrence decreases with increasing temperature (same range of temperatures than those studied). Indeed, <c>-component loop nucleation is known to depend on the amount of alloying elements rejected into the matrix from the dissolution of precipitates that is enhanced by the temperature (Idrees, 2013; Idrees *et al.*, 2015). In the case of

CP Ti grade 2, the amount of alloying elements is very low and it can be considered that at high temperature, vacancy thermal emission mechanism might have occurred at the early stage of nucleation of the loops causing elimination of vacancy type loops after nucleation, resulting in lower density at 430°C 0.6 dpa than at 300°C (Idrees, 2013). As for <a>-type dislocation loops, this phenomenon is reduced after an irradiation at low flux and further experiments seem necessary to understand it.

Conclusion

In this study, the radiation-induced loops in the CP Ti grade 2 and their evolution was observed and analysed. Ti^{2+} ions (with energy of 6 MeV and use of 0.8 μm Al degrader) were successfully used in order to simulate the microstructures described in the literature after neutron irradiation. The hardened microstructure with a high density of small defects was observed at the temperature of 300°C. Irradiation conducted at 430°C reproduces the higher temperature microstructure with less numerous and less hardening bigger defects. Regardless of considered irradiation conditions excepted for 0.6 dpa high flux, <a>-type dislocation loops were observed as expected, but also numerous <c>-component loops. At 300°C, black dots are observed but not quantified according to their small size.

The influence of different irradiation parameters (temperature, dose and flux) on the defect microstructure has been characterized:

- No influence of dose and flux is observed at 300°C for <a>-type and <c>-component loops.
- By increasing temperature (300°C➔430°C), number density of <a>-type dislocation loops decreases and their size is larger. In the case of the <c>-component loops, linear density and size are quite similar in both irradiation temperature conditions after irradiation at a dose of 3 dpa. Wavy aspect of these loops is noted at 430°C. Presence of <c>-component loops can be explained by the DAD (Diffusion Anisotropy Difference) model.
- Influence of dose and flux is observed at 430°C for <a>-type and <c>-component loops. <c>-component loops are less numerous at 0.6 dpa high flux. As regards <a>-type dislocation loops, their presence is only noticed at 0.6 dpa low flux and 3 dpa high flux.

Acknowledgements

The authors acknowledge the support of the French National Research Agency (ANR), under grant ANR-12-RMNP-0005 (project TESAMI, meaning Titanium and Its Alloys under Irradiation) and the partners of the project: DCNS, CEA, AREVA TA, TIMET, VALTIMET, EVEA, ICB and SUBATECH.

The authors would like to warmly thank the staff of JANNUS facility for their assistance during ion irradiations. The authors are indebted to B. Arnal and T. Vandenberghe (CEA-DEN-DMN-SRMA) for their help in the area of TEM examinations.

References

Beck, L., Serruys, Y., Miro, S. *et al.* (2015). Ion irradiation and radiation effect characterization at the JANNUS-Saclay triple beam facility. *J. Mater. Res.* **30**, 1183–1194.

Crozier, P.A. (1990). Measurement of inelastic electron scattering cross sections by electron energy-loss spectroscopy. *Philos. Magaz.* **61**, 311–336.

Doriot, S., Verhaeghe, B., Béchade, J.-L. *et al.* (2014). Microstructural Evolution of M5TM7 Alloy Irradiated in PWRs up to High Fluences – Comparison with Other Zr-based Alloys, vol. **STP 1543**, pp. 759–799. Robert Comstock and Pierre Barberis.

Dubinko, V., Turkin, A., Abyzov, A. & Griffiths, M. (2006). Modeling of the simultaneous evolution of vacancy and interstitial dislocation loops in hcp metals under irradiation. *J. ASTM Int.* **3**, 157–174.

Egerton, R.F. (1996). *Electron Energy-Loss Spectroscopy in the Electron Microscope*, 2nd edn. Plenum Press, New York.

Garner, F.A. (2012). 4.02 Radiation damage in austenitic steels. *Comprehensive Nuclear Materials*, vol. 4: Radiation Effects in Structural and Functional Materials for Fission and Fusion Reactors (ed. by Rudy J. M. Konings), pp. 33–95. Elsevier, Amsterdam.

Gilbon, D. & Simonot, C. (1994). *Effect of Irradiation on the Microstructure of Zircaloy-4* (ed. by M. Garde & E. R. Bradley), vol. ASTM STP 1245, pp. 521–548. Philadelphia.

Gilbon, D., Soniak, A., Doriot, S. & Mardon, J.-P. (2000). Irradiation Creep and Growth Behavior, and Microstructural Evolution of Advanced Zr-based Alloys, vol. ASTM STP 1354, pp. 51–73. West Conshohocken.

Griffiths, M. (1988). A review of microstructure evolution in zirconium alloys during irradiation. *J. Nucl. Mater.* **159**, 190–218.

Griffiths, M. (1991). Microstructure evolution in h.c.p. metals during irradiation. *Philos. Magaz. A* **63**, 835–847.

Griffiths, M. (1993a). Evolution of microstructure in hcp metals during irradiation. *J. Nucl. Mater.* **205**, 225–241.

Griffiths, M. (1993b). HVEM study of the effects of alloying elements and impurities on radiation damage in Zr-alloys. *J. Nucl. Mater.* **205**, 273–283.

Griffiths, M., Faulkner, D. & Styles, R.C. (1983). Neutron damage in α-titanium. *J. Nucl. Mater.* **119**, 189–207.

Hengstler-Eger, R.M., Baldo, P., Beck, L. *et al.* (2012). Heavy ion irradiation induced dislocation loops in AREVA's M5 alloy. *J. Nucl. Mater.* **423**, 170–182.

Idrees, Y. (2013). *Microstructural evolution in Zr and Zr alloy Excel under ion irradiation*. PhD Thesis, Queen's University, Kingston, Ontario, Canada.

Idrees, Y., Francis, E.M., Yao, Z., Korinek, A., Kirk, M.A., Sattari, M., Preuss, M. & Daymond, M.R. (2015). Effects of alloying elements on the formation of <c>-component loops in Zr alloy Excel under heavy ion irradiation. *J. Mater. Res.* **30**, 1310–1334.

Kozhevnikov, O.A., Nesterova, E.V., Rybin, V.V. & Yarmolovich, I.I. (1999a). Influence of neutron irradiation on deformability and fracture micromechanisms of titanium α-alloys. *J. Nucl. Mater. 271--272*, 472–477.

Kozhevnikov, O.A., Nesterova, E.V., Rybin, V.V. & Yarmolovich, I.I. (1999b). Mechanical properties, fine structure, and micromechanisms

of fracture in titanium α-alloys irradiated with neutrons. *Metal Sci. Heat Treat.* **41**, 412–416.

Lee, C.W., Ikematsu, Y. & Shindo, D. (2002). Measurement of mean free path for inelastic electron scattering of Si and SiO2. *J. Electr. Microsc.* **51**, 143–148.

Leguey, T., Baluc, N., Schäublin, R. & Victoria, M. (2001). Structure/mechanics relationships in proton irradiated pure titanium. *J. Nucl. Mater.* **307–311**, 696–700.

Mansur, L.K. (1978). Correlation of neutron and heavy-ion damage: II. The predicted temperature shift if swelling with changes in radiation dose rate. *J. Nucl. Mater.* **78**, 156–160.

Mitchell, D.R.G. (2006). Determination of mean free path for energy loss and surface oxide film thickness using convergent beam electron diffraction and thickness mapping: a case study using Si and P91steel. *J. Microsc.* **224**, 187–196.

Nakafuji, A., Murakami, Y. & Shindo, D. (2001). Effect of diffraction condition on mean free path determination by EELS. *J. Electr. Microsc.* **50**, 23–28.

Nastar, M. & Soisson, F. (2012). 1.18 Radiation-induced segregation. *Comprehensive Nuclear Materials*, vol. 1: Basic Aspects of Radiation Effects in Solids/Basic Aspects of Multi-Scale Modeling (ed. by Rudy J. M. Konings), pp. 471–496. Elsevier, Amsterdam.

Northwood, D.O., Gilbert, R.W., Bahen, L.E. *et al.* (1979). Characterization of neutron irradiation damage in zirconium alloys – an international 'Round-Robin' experiment. *J. Nucl. Mater.* **79**, 379–394.

Ohshima, K., Kaneko, K., Fujita, T. & Horita, Z. (2004). Determination of absolute thickness and mean free path of thin foil specimen by zeta-factor method. *J. Electr. Microsc.* **53**, 137–142.

Onimus, F. & Béchade, J.-L. (2012). 4.01 Radiation Effects in Zirconium Alloys. *Comprehensive Nuclear Materials,* vol. 4:Radiation Effects in Structural and Functional Materials for Fission and Fusion Reactors (ed. by Rudy J. M. Konings), pp. 1–31. Elsevier, Amsterdam.

Pokor, C., Brechet, Y., Dubuisson, P., Massoud, J.-P. & Barbu, A. (2004). Irradiation damage in 304 and 316 stainless steels: experimental investigation and modeling. *J. Nucl. Mater.* **326**, 19–29.

Renault-Laborne, A., Gavoille, P., Malaplate, J., Pokor, C. & Tanguy, B. (2015). Correlation of radiation-induced changes in microstructure/microchemistry, density and thermo-electric power of type 304L and 316 stainless steels irradiated in the Phénix reactor. *J. Nucl. Mater.* **460**, 72–81.

Serruys, Y., Trocellier, P., Miro, S. *et al.* (2009). JANNUS: a multi-irradiation platform for experimental validation at the scale of the atomistic modeling. *J. Nucl. Mater.* **386–388**, 967–970.

Simonot, C. (1995). Evolutions microstructurales des alliages de zirconium sous irradiation: Liens avec le phénomène de croissance. PhD Thesis.

Tähtinen, S., Moilanen, P. & Singh, B.N. (2007). Effect of displacement dose and irradiation temperature on tensile and fracture toughness properties of titanium alloys. *J. Nucl. Mater.* **367–370**, 627–632.

Tournadre, L., Onimus, F., Béchade, J.-L., Gilbon, D., Cloué, J.-M., Mardon, J.-P. & Feaugas, X. (2013). Toward a better understanding of the hydrogen impact on the radiation induced growth of zirconium alloys. *J. Nucl. Mater.* **441**, 222–231.

Tournadre, L., Onimus, F., Béchade, J.-L. *et al.* (2012). Experimental study of the nucleation and growth of c-component loops under charged particle irradiations of recristallized Zircaloy-4. *J. Nucl. Mater.* **425**, 76–82.

Was, G.S. (2007). *Fundamentals of Radiation Materials Science: Metals and Alloys*. Springer, Berlin.

Was, G.S. & Averback, R.S. (2012). 1.07 Radiation damage using ion beams. *Comprehensive Nuclear Materials*, vol. 1: Basic Aspects of Radiation Effects in Solids/Basic Aspects of Multi-Scale Modeling (ed. by Rudy J. M. Konings), pp. 195–221. Elsevier, Amsterdam.

Wasz, M.L., Brotzen, F.R., McLellan, R.B. & Griffin, A.J. (1996). Effect of oxygen and hydrogen on mechanical properties of commercial purity titanium. *Int. Mater. Rev.* **41**, 1–12.

Woo, C.H. (1988). Theory of irradiation deformation in non-cubic metals: effects of anisotropic diffusion. *J. Nucl. Mater.* **159**, 237–256.

Woo, C.H. (2000). Defect accumulation behaviour in hcp metals and alloys. *J. Nucl. Mater.* **276**, 90–103.

Yan, C., Wang, R., Wang, Y., Wang, X. & Bai, G. (2015). Effects of ion irradiation on microstructure and properties of zirconium alloys – a review. *Nucl. Eng.Tech.* **47**, 323–331.

Zinkle, S.J. (2012). 1.03 Radiation-induced effects on microstructure. *Comprehensive Nuclear Materials*, vol. 1: Basic Aspects of Radiation Effects in Solids/Basic Aspects of Multi-Scale Modeling (ed. by Rudy J. M. Konings), pp. 65–98. Elsevier, Amsterdam.

Zinkle, S.J., Maziasz, P.J. & Stoller, R.E. (1993). Dose dependence of the microstructural evolution in neutron-irradiated austenitic stainless steel. *J. Nucl. Mater.* **206**, 266–286.